

Properties of the high-mass star forming region IRAS 22475+5939

Xiao-Lan Liu^{1,2} and Jun-Jie Wang¹

¹ National Astronomical Observatories, Chinese Academy of Sciences, Beijing 100012, China;
liuxiaolan10@mails.gucas.ac.cn

² Graduate University of Chinese Academy of Sciences, Beijing 100049, China

Received 2012 February 7; accepted 2012 March 23

Abstract IRAS 22475+5939 has been well studied by previous astronomers, but we can still discover new characteristics about it, using the first observations of the lines from CO $J=2-1$, $^{13}\text{CO } J=2-1$ and $^{13}\text{CO } J=3-2$ by the KOSMA 3m telescope. The mapping of the intensity ratio of $^{13}\text{CO } J=3-2$ and $^{13}\text{CO } J=2-1$ shows that the distribution of the temperature has two peaks, neither of which coincide with the IRAS 22475+5939 source or the center of the HII region, but rather are located at the edge of the HII region. Overlays of the Spitzer IRAC 8 μm with CO contours indicate that they are associated with each other and that the strongest polycyclic aromatic hydrocarbon (PAH) emission is at the IRAS 22475+5939 source position. The IRAS LRS spectrum at 7 $\mu\text{m} \sim 23 \mu\text{m}$ and the PHT-s spectrum at 2 $\mu\text{m} \sim 12 \mu\text{m}$ of the IRAS 22475+5939 source also exhibit strong PAH emission characteristics in the main PAH bands. The diversity of the PAH family should be responsible for the plateaus in the PAH emission in the PHT-s and IRAS-LRS spectra. Analysis and modeling in the infrared bands suggest that IRAS 22475+5939 is more likely to be a class I young stellar object. Where this is the case, the star is likely to have a temperature of $T_{\text{eff}} \sim 9995.8 \text{ K}$, mass $\sim 15.34 M_{\odot}$, luminosity $\sim 1.54 \times 10^4 L_{\odot}$ and age $\sim 1.54 \times 10^4 \text{ yr}$. The model shows that circumstellar disc emission is important for wavelengths between 1 and 10 μm , otherwise, the envelope fluctuates for $\lambda > 10 \mu\text{m}$. Bipolar outflow is confirmed in the molecular cloud, and the excited star of the HII region could be the driving source of the outflow. High resolution is required for better results.

Key words: ISM: jets and outflow — ISM: molecular — ISM: kinematical and dynamics — star formation

1 INTRODUCTION

Research into massive star formation has attracted significant attention in recent years, but the mechanism of how massive stars form is still debatable. Researchers are investigating whether this is through the process similar to that for low mass stars, i.e., disc accretion and driven molecular outflows (Shu et al. 1987), or alternative scenarios such as the coalescence of low mass stars (Bonnell et al. 1998). However, recent observations have shown that outflows are common in massive star forming regions (Zhang et al. 2001) and it is now almost clear that stars at least up to late-O spectral types form primarily through disc accretion (Varricatt 2012). HII regions will form when the

massive stars ionize their surroundings and provide information about massive star formation within molecular clouds (Heyer et al. 1989; Churchwell 2002). Therefore, the forming stars will have a large influence on their surrounding environment during the evolution processes. This is an indirect way of studying the properties exhibited by star forming regions in order to know more about how massive stars form.

IRAS 22475+5939 has been detected in the sharply defined HII region S146 (Zuckerman & Evans 1974). The distance of IRAS 22475+5939 from us is about 4.7 kpc (Henkel et al. 1986). Eiroa et al. (1981) believed that S146 was excited by an IRS 1 located at position $\alpha(B1950) = 22^{\text{h}}47^{\text{m}}29^{\text{s}}.7$, $\delta(B1950) = +59^{\circ}38'55'' \pm 7$ at $2.2 \mu\text{m}$ and $\alpha(B1950) = 22^{\text{h}}47^{\text{m}}29^{\text{s}}.5$, $\delta(B1950) = +59^{\circ}39'01'' \pm 3$ at $0.9 \mu\text{m}$. Blair et al. (1978) found an H_2O maser associated with IRAS 22475+5939. A 2MASS source 22492900+59545600 ($\alpha = 22^{\text{h}}49^{\text{m}}29^{\text{s}}.06$, $\delta = +59^{\circ}54'55''.7$, J2000) was detected by Wang (1997). Felli & Harten (1981) showed this source is a bipolar outflow with optical and 6 cm emissions. The bipolar molecular outflow was also confirmed from surveys of CO $J=1-0$ (Yang & Wu 1998), CO $J=2-1$ (Jiang et al. 2001) and CO $J=3-2$ (Wu et al. 2005) and Jiang et al. (2001) thought a massive star was forming in the molecular cloud. Guan et al. (2008) mapped a survey of massive CO cores with CO, ^{13}CO and ^{18}CO $J=1-0$ lines. The contour of ^{13}CO $J=1-0$ was found to be associated with MSX $8 \mu\text{m}$ emission (Guan & Wu 2008). The IRAS-LRS (low resolution spectra) spectrum was analyzed by Jourdain de Muizon et al. (1990), Volk et al. (1991) and Chen et al. (1995). The LRS spectrum shows strong [NeII] ($12.8 \mu\text{m}$), [NeIII] ($15.5 \mu\text{m}$), [SIII] ($18.7 \mu\text{m}$) and emission from polycyclic aromatic hydrocarbons (PAHs) ($7.7 \mu\text{m}$, $8.6 \mu\text{m}$, $11.3 \mu\text{m}$), as well as a silicate absorption feature at $9.7 \mu\text{m}$ (Jourdain de Muizon et al. 1990; Volk et al. 1991; Chen et al. 1995).

In this paper, we show the existence of the outflow and discuss the properties in the observed region. ^{13}CO is optically thin and can trace the internal region of the molecular core, and the intensity ratio $R_{132/21}$ (ratio of ^{13}CO $J=3-2$ and ^{13}CO $J=2-1$) contains information about the temperature distribution in the molecular cloud. The mid-infrared emission at $8 \mu\text{m}$ is thought to be from small dust grains and PAHs, and is excited by UV radiation leaking from the HII regions (Leger & Puget 1984; Deharveng et al. 2003, 2005). We also use the Stokes I image from the observations for the 1.4 GHz NRAO VLA Sky Survey (NVSS) to trace the HII region in order to better understand the relationship between the molecular cloud, the intensity ratio and the HII region. We describe the observation in Section 2, the results and a discussion of the properties are in Section 3, and in Section 4 we provide a conclusion.

2 OBSERVATIONS AND DATA REDUCTION

2.1 The Observed Data

We carried out observations toward the IRAS 22475+5939 ($\alpha = 22^{\text{h}}49^{\text{m}}29^{\text{s}}.4$, $\delta = +59^{\circ}54'54''.00$, J2000) source in the CO $J=2-1$, ^{13}CO $J=2-1$ and ^{13}CO $J=3-2$ lines using the KOSMA 3 m telescope at Gornergrat, Switzerland in 2004 April. The half-power beam widths of the telescope at observing frequencies 230.538 GHz, 220.399 GHz and 330.588 GHz are $130''$, $130''$ and $80''$, respectively. The pointing and tracking accuracy is better than $10''$, and the DSB receiver noise temperature is about 120 K. The medium and variable resolution acousto-optical spectrometers have 1501 and 1601 channels, and the channel widths of 248 MHz and 544 MHz correspond to velocity resolutions of 0.21 km s^{-1} and 0.29 km s^{-1} , respectively. The beam efficiency is 0.68 at 230 GHz and 220 GHz, but 0.72 at 330 GHz and 345 GHz. The forward efficiency is 0.93, and the $80''$ resolution of the $J=3-2$ data was convolved to $130''$ with an effective beam size of $\sqrt{(130^2 - 80^2)} = 102''$. A correction for the line intensities to the main beam temperature scale was made using the formula $T_{\text{mb}} = (F_{\text{eff}}/B_{\text{eff}} * T_A^*)$. The data were reduced by the software CLASS (Continuum and Line Analysis Single-Disc Software) and GREG (Grenoble Graphic).

2.2 Archived Data

Spitzer IRAC 8 μm imaging is available toward the direction of IRAS 22475+5939 at an angular resolution of $\sim 2''$. S146 was clearly detected by the 1.4 GHz signal of NVSS. Its resolution is $45''$ and limiting peak source brightness is about $2.5 \text{ mJy beam}^{-1}$. We have compiled the SED for the IRAS 22475+5939 source using near-IR (*JHK*) flux from the 2MASS All-Sky Point Source Catalog (PSC), four mid-IR MSX bands from the Midcourse Space Experiment Catalog 6 (MSXC6) and IRAS data from the IRAS PSC v2.1. The IRAS LRS spectrum is obtained from the LRS database at the University of Calgary¹ (Hodge et al. 2004; Kwok et al. 1997). The LRS was a slitless spectrometer and well-suited to point sources, whereas confusion arises in the case of extended sources. Two wavelength channels are recorded simultaneously: band 1 (7.7 – 13.4 μm) and band 2 (11.0 – 22.6 μm). The wavelength resolution $\lambda/\Delta\lambda$ varies between 10 and 60; it increases with wavelength inside each wavelength band, with the resolution being systematically lower in band 2 than in band 1. The PHT-s instrument consists of a dual grating spectrometer with two 64-element arrays that span the 2.5 – 4.9 μm and 5.8 – 11.6 μm spectral regions. The auto analysis result produced by the off-line processing (OLP) from the ISO Data Archive (IDA) is available (Hodge et al. 2004; Lemke et al. 1996).

3 RESULTS AND DISCUSSION

3.1 The Outflow

3.1.1 The molecular spectral lines

Figure 1 shows the spectra and channel maps of CO $J=2-1$, $^{13}\text{CO } J=2-1$ and $^{13}\text{CO } J=3-2$. The spectra are at positions $(-1, 0)$. Each spectrum shows a broad width as well as almost the same V_{LSR} and shape. The spectra shown are the strongest for $^{13}\text{CO } J=2-1$ and $^{13}\text{CO } J=3-2$. The optically thick line CO $J=2-1$ does not have a Gaussian shape because it has wings. The blue and red wings are symmetrical. Table 1 presents observational parameters of the IRAS 22475+5939 source. The ranges of the FW come from the position-velocity (P-V) diagram, which shows that high-velocity gas exists.

Table 1 Observed Physical Parameters of the IRAS 22475+5939 Source

Name	T_{mb} (K)	FWHM (km s^{-1})	FW (km s^{-1})	V_{LSR} (km s^{-1})
CO ($J=2-1$)	11.20	4.99 ± 0.03	12.37	-49.60 ± 0.01
$^{13}\text{CO } (J=2-1)$	3.02	3.90 ± 0.08	6.33	-49.80 ± 0.04
$^{13}\text{CO } (J=3-2)$	2.55	4.79 ± 0.17	7.87	-49.69 ± 0.07

3.1.2 The outflow and its physical parameters

We show the outflow and its corresponding P-V diagram in Figure 2. The integrated ranges of the blue and red wings are determined by the P-V diagram and Gaussian fit. We find that they overlap each other, which is likely to be because they are in the direction of sight or the resolution of the telescope is too low to identify the direction of the outflows. IRAS 22475+5939, as well as its associated H_2O maser, is almost in the center of the wings. Perhaps IRAS 22475+5939 is the driving source of the outflow. The physical parameters are presented in Table 2. Assuming it is in local thermodynamic equilibrium (LTE) and that CO in the outflow is optically thin, we can calculate the

¹ See <http://www.astro.wisc.edu/protostars>

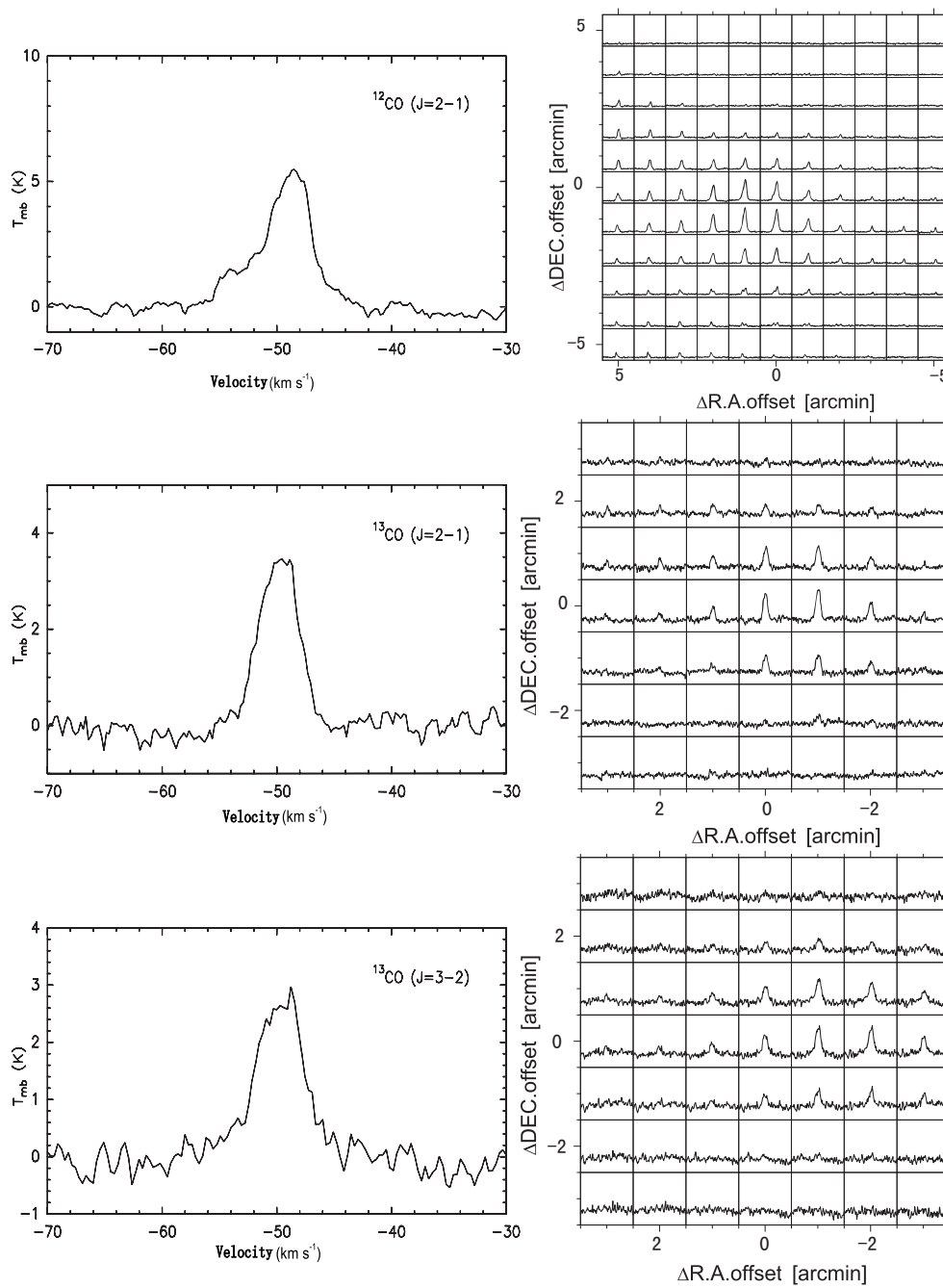


Fig. 1 Left: the spectra of $\text{CO} (J=2-1)$, $^{13}\text{CO} (J=2-1)$ and $^{13}\text{CO} (J=3-2)$ at a position of $(-1, 0)$. Right: channel maps of the corresponding isotopes.

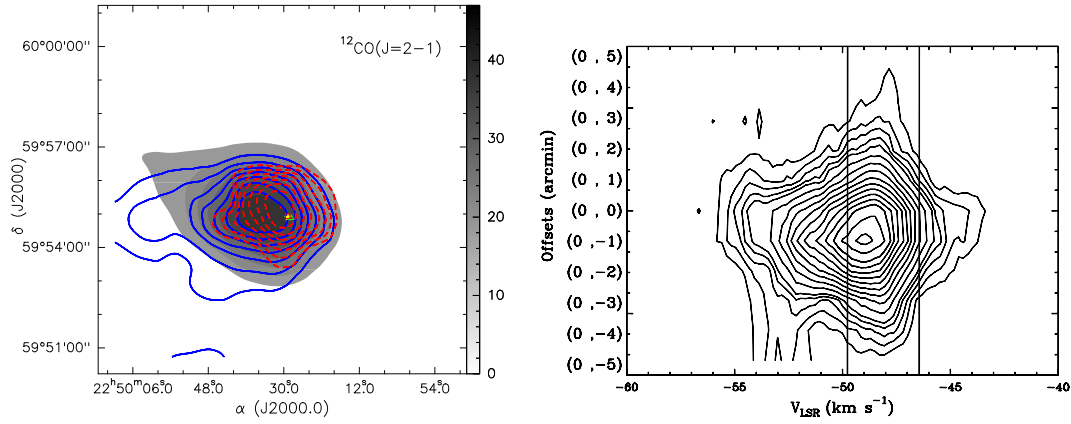


Fig. 2 *Left panel:* outflow contours of CO ($J=2-1$); the integrated ranges in the blue and red wings are $-55.78 \text{ km s}^{-1} \sim -50.80 \text{ km s}^{-1}$ and $-46.05 \text{ km s}^{-1} \sim -43.41 \text{ km s}^{-1}$, respectively. The contour levels are 30% \sim 90% of each wing's peak value. The star is IRAS 22475+5939, the triangle is the H_2O maser, and the square is the 2MASS source 22492900+59545600. *Right panel:* P-V diagram. The contour levels are 0.7 \sim 3 by 0.6 K, 3 \sim 12 by 1.0 K and 12 \sim 20 by 1.5 K. The two vertical lines indicate the beginning of the blue and red wings, respectively.

Table 2 The Physical Parameters of the Outflow

Name	Wing	$N(\text{H}_2)$ (10^{20} cm^{-2})	M (M_\odot)	t_d (10^5 yr)	\dot{M} ($10^{-6} M_\odot \text{ yr}^{-1}$)
22475 + 5939	blue	1.00	278.79	5.37	3.86
	red	0.15	26.63	3.25	0.80
Name	Wing	F ($M_\odot \text{ km s}^{-1} \text{ yr}^{-1}$)	P ($M_\odot \text{ km s}^{-1}$)	E (10^{46} erg)	L_{Mech} (L_\odot)
22475 + 5939	blue	1.93×10^{-3}	1028.74	7.59	1.17
	red	3.99×10^{-4}	129.699	1.26	1.23

column density of the outflow using the formula below (Scoville et al. 1986) under the assumption that $N(\text{CO})/N(\text{H}_2) \approx 10^{-4}$ (Dickman 1978)

$$N = 10^5 \times \frac{3k^2}{4h\pi^3\mu^2\nu^2} \exp\left(\frac{h\nu J}{2kT_{\text{ex}}}\right) \frac{T_{\text{ex}} + h\nu/6k(J+1)}{\exp(-h\nu/kT_{\text{ex}})} \times \int \frac{\tau}{1 - e^{-\tau}} T_{\text{mb}} dv, \quad (1)$$

where T_{ex} is the excitation temperature, J is the lower level of the transition and $\mu = 0.112 D$.

The other physical parameters are from the formulas given below (Xu & Wang 2010):

$$M = um_{\text{H}_2}SN(\text{H}_2)/2 \times 10^{33}, \quad (2)$$

$$P = MV, \quad (3)$$

$$E = MV^2, \quad (4)$$

$$t_d = R/V, \quad (5)$$

$$F = P/t_d, \quad (6)$$

$$\dot{M} = P/t_d v_w, \quad (7)$$

$$L_{\text{Mech}} = E/t_d, \quad (8)$$

where M is the mass of the outflow, and t_d , P , E , V , R , F and L_{Mech} are the dynamic time, momentum, energy, mean velocity of gas relative to V_{LSR} , size of the wings, driving force and mechanical luminosity, respectively. The mean atomic weight of the gas is $u = 1.36$ and S is the area of the outflow. From these parameters, we can see that the outflow is massive and energetic compared with the low-mass stars, so we further validate that it is possible to have massive stars forming in this region. At the same time, through the outflow and its parameters, we find that the blue outflow is far larger than the red one, and that both are elongated from east to west, which is very similar to the $^{13}\text{CO } J = 3 - 2$ molecular core that is presented later. The explanation for this is that the surrounding gas might mix with the blue wing, but we cannot be sure because of the low resolution of the telescope.

3.2 The Molecular Core

Figure 3 shows the structure of the molecular core. The integrated range is determined by the P-V diagram and the Gaussian fit due to the relatively large noise. It is more accurate than the one determined by each of the two methods separately. In the diagrams, we find that the core structure from $^{13}\text{CO } J = 3 - 2$ is elongated from east to west, but almost round from the transitions $\text{CO } J = 2 - 1$ and $^{13}\text{CO } J = 2 - 1$. IRAS 22475+5939 and the H_2O maser coincide with the peak of the cores. We also calculate the core's physical parameters by the expressions (Garden et al. 1991) under the assumption of LTE:

$$T_{\text{ex}}(\text{CO}) = \frac{h\nu}{k} \left(\ln \left(1 + \frac{h\nu}{k} \left[\frac{T_{\text{mb}}}{f} + \frac{h\nu/k}{\exp(h\nu/kT_{\text{bg}}) - 1} \right]^{-1} \right) \right)^{-1}, \quad (9)$$

$$\tau(^{13}\text{CO}) = -\ln \left\{ 1 - \frac{kT_{\text{mb}}}{h\nu} \left[\frac{1}{\exp(h\nu/kT_{\text{ex}}) - 1} - \frac{1}{\exp(h\nu/kT_{\text{bg}}) - 1} \right]^{-1} \right\}, \quad (10)$$

where $T_{\text{bg}} = 2.732\text{ K}$ is the temperature of the cosmic background radiation, and f is the beam filling factor. Here we assume $f = 1$ and $\tau(\text{CO})/\tau(^{13}\text{CO}) = [\text{CO}]/[^{13}\text{CO}] = 89$ (Lang 1980). We can use another method to calculate the optical depths

$$\frac{T_{\text{mb}}(\text{CO})}{T_{\text{mb}}(^{13}\text{CO})} = \frac{1 - \exp[-\tau(\text{CO})]}{1 - \exp[-\tau(^{13}\text{CO})]}. \quad (11)$$

The two calculated values are summarized in Table 3, and by comparing them we find that the values of the two methods are almost same within the error. Therefore, we can draw a conclusion that our assumptions are reasonable and the abundance ratio $[\text{CO}]/[^{13}\text{CO}]$ in this region is almost the same as in our solar system. The physical parameters of the core are shown in Table 4. From the figures and tables, we can find that the core is isolated and massive, which can provide the environment for the formation of high-mass stars.

Table 3 Calculated Results of the Optical Depth from Using the Two Methods

Name	τ_1	τ_2
$^{13}\text{CO}(J = 2 - 1)$	0.28	0.28

τ_1 is derived from the first method and τ_2 is from the second method.

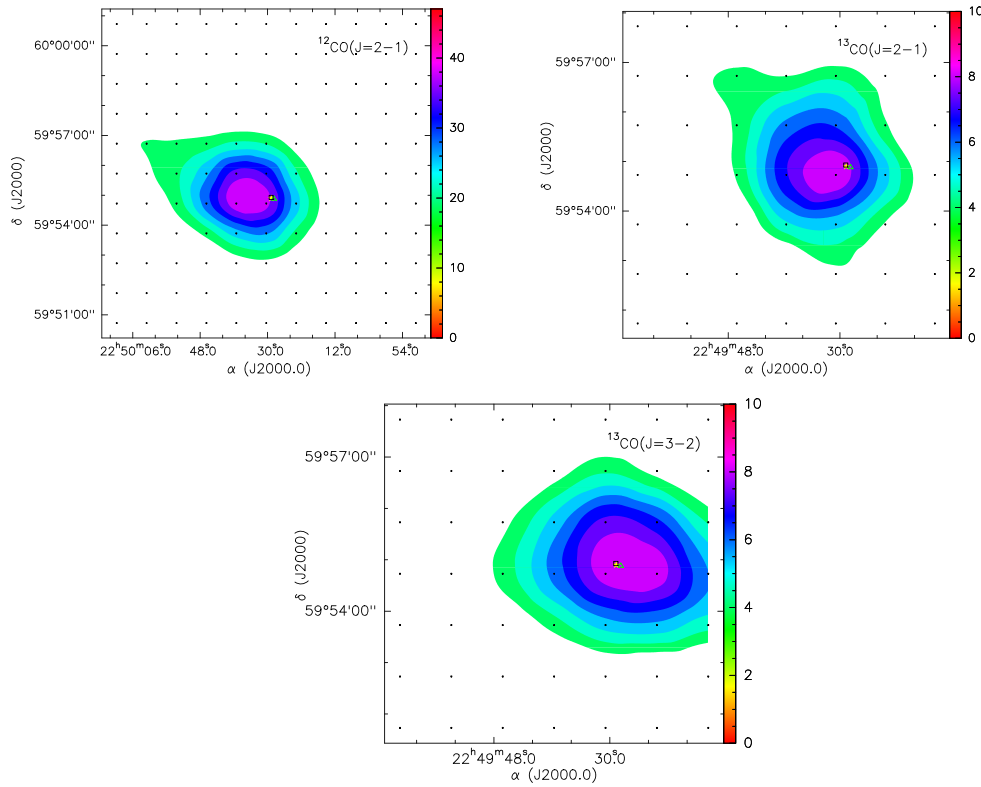


Fig. 3 Integrated intensity diagrams of the core emission. In each map, the integrated range is from -50.80 km s^{-1} to -46.05 km s^{-1} . The contour levels are 30% to 90% of the peak value.

Table 4 The Physical Parameters of the Core

Name	T_{ex} (K)	τ	$N(\text{CO } J = 2 - 1)$ (10^{18} cm^{-2})	$N(\text{H}_2)$ (10^{22} cm^{-2})	M ($10^3 M_{\odot}$)
IRAS 22475 + 5939	17.35	24.92	1.03	1.03	3.56

3.3 The Intensity Ratio $R_{I_{32/21}}$

Figure 4 gives the contours of ^{13}CO and the intensity ratio $R_{I_{32/21}}$ superimposed on the 1.4 GHz NVSS grayscale diagram which can trace the structure of the radio source. Here we can identify that the radio source is an HII region (Lockman 1989). The intensity ratio indicates the gas temperature distribution in the region (Qin et al. 2008). From Figure 4, we can find that the morphology of the intensity ratio map is similar to a triangle and has three peaks. The peaks are not in the center of the molecular cloud core; the biggest peak is in the northwest, about $2'$ away from the center. Its value is $\sim 2.12 > 1$, which is bigger than the (< 1) value detected in Cepheus B (Beuther et al. 2000). This may be related to the HII regions (Wilson et al. 1997). The second peak and the third peak are in the southwest and east directions, respectively, and all three are at the edge of the HII region. This shows the temperature at the edge is higher than at the center. Perhaps the hot gas of the molecular cloud was pushed away to the edge and heated by the HII region. This explanation can be supported by the

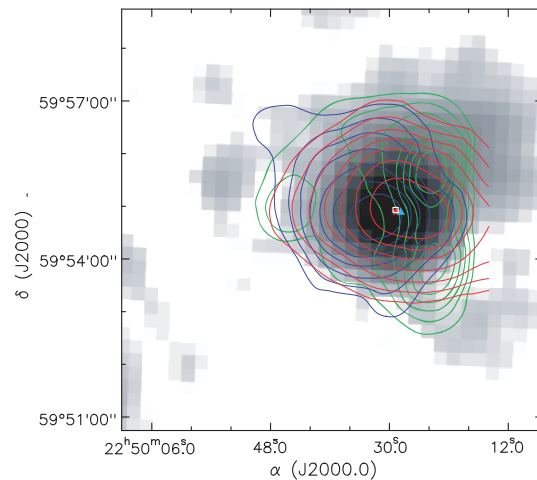


Fig. 4 The grayscale shows the 1.4 GHz NVSS image. The intensity ratio $R_{132/21}$ is the green contour, and the blue and red contours are the integrated intensity maps of ^{13}CO ($J=2-1$) and ^{13}CO ($J=3-2$), respectively. The star is IRAS 22475+5939, the triangle is the H_2O maser, and the square is the 2MASS source 22492900+59545600.

distribution of the HII region and the molecular core. Additionally, we find that higher J values in ^{13}CO can trace the warmer region, and that the center of the molecular core coincides with that of the HII region.

3.4 Polycyclic Aromatic Hydrocarbons (PAHs)

Figure 5 shows the superposition diagrams of contours of the CO isotopes and the CO outflow from the Spitzer 8 μm emission. The Spitzer IRAC 8 μm emission is primarily due to the 7.7 μm and 8.6 μm PAH features. The grayscale diagram shows the distribution of PAHs in the HII region. We can see that the strongest PAH emission coincides with the IRAS 22475+5939 source, which shows that the PAH emission is probably excited by the UV radiation from IRAS 22475+5939.

Figure 6 shows the LRS and PHT-s spectra, spanning the wavelengths 7.7 – 23 μm and 2 – 12 μm , respectively. They are dominated by PAH emission features at the so-called unidentified infrared bands (3.3, 6.2, 7.7, 8.6, 11.2 μm) and weaker bands² (Peeters 2011). The PHT-s spectrum shows the narrow and strongest emission at 7.6 μm at the wavelength range 2 – 12 μm , and an absorption at 9.7 μm , but the strongest emission for the LRS is at 12.0 μm at band 1. This is more believable for the PHT-s due to their higher resolution than the results of the LRS. A broad emission plateau at 16.4 – 17.4 μm may also be identified from the low resolution or the diverse PAH family. Jourdain de Muizon et al. (1990) pointed out that the prominent emissions at 12.8, 15.55 and 18.7 μm are [NeII], [NeIII] and [SIII] lines, respectively.

3.5 The Spectral Energy Distribution

The 2MASS, MSX and IRAS data are used to construct the SED of the IRAS 22475+5939 source. Color correction is applied to the IRAS data using the correction factors given in the point source

² This includes bands at 3.4, 3.5, 5.25, 5.75, 6.0, 6.6, 6.9, 7.2–7.4, 8.2, 10.5, 10.8, 11.0, 12.0, 13.5, 14.2, 15.8, 16.4, 16.6, 17.0, 17.4, 17.8 and 19.0 μm .

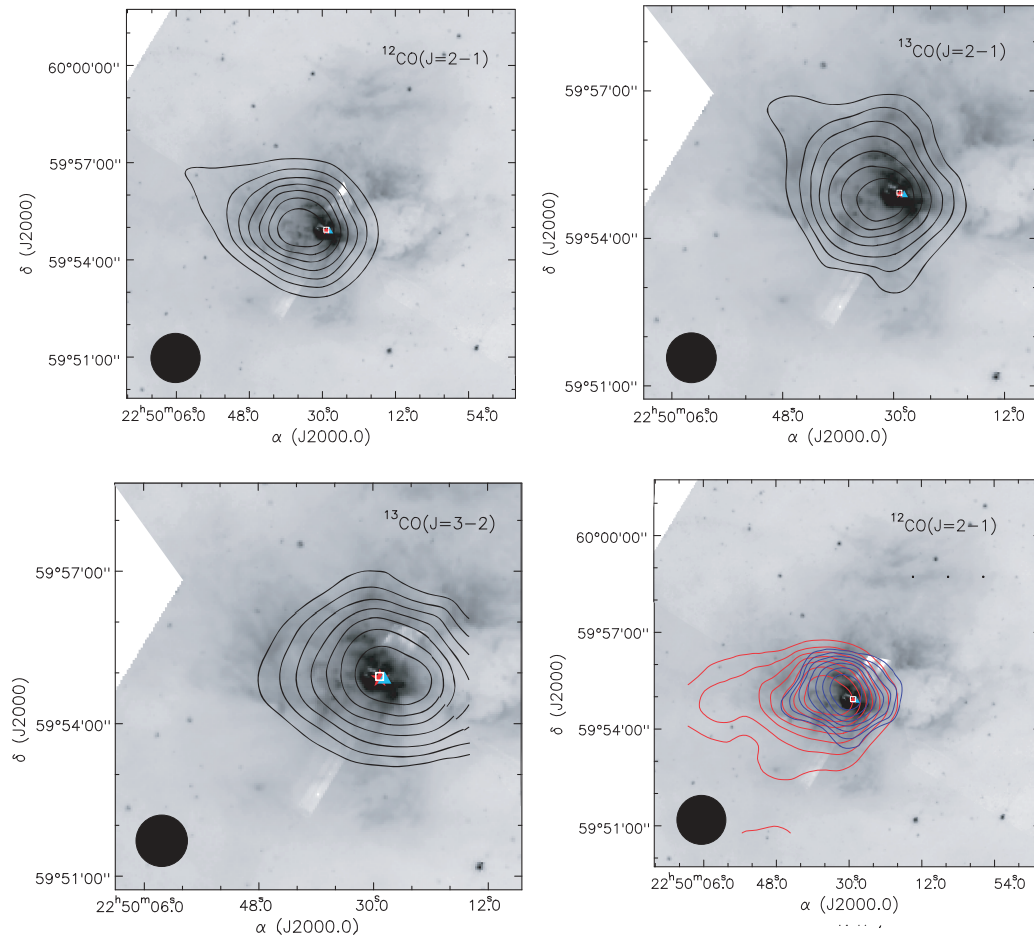


Fig. 5 The molecular cores from the transitions $\text{CO} (J=2-1)$, $^{13}\text{CO} (J=2-1)$ and $^{13}\text{CO} (J=3-2)$ (top left, top right, bottom left) and the outflow of $\text{CO} (J=2-1)$ emission (bottom right) overlaid on the grayscale Spitzer $8\ \mu\text{m}$ emission. The synthesized beam size ($\sim 1'$) of the KOSMA 3 m telescope is shown in the lower left-hand corner of each panel.

catalog (Beichman et al. 1988). The SED fitting tool of Robitaille et al. (2007) is available on-line to model the SED. The SED plot is shown in Figure 7 and its fitting parameters are in Table 5. We derived a mass, luminosity and temperature of $15.34 M_{\odot}$, $1.54 \times 10^4 L_{\odot}$ and 9995.8 K, respectively, from the fit, and the average foreground extinction is ~ 4.53 . From the SED and the active accreting mass, IRAS 22475+5939 is probably a class I protostar.

We have also indicated the differing flux components, which make up the model young stellar object (YSO) spectrum (right panel of Fig. 7). In this case, the total flux is indicated as black, the stellar flux as blue, the stellar photospheric flux is shown as the dashed line (this is the flux prior to reddening by circumstellar dust), the disc flux as green, the scattered flux as pink, the envelope flux as red and the thermal flux as orange. Unless otherwise stated, the results include the effects of circumstellar extinction, but not of interstellar extinction. They also assume a representative distance of 1 kpc.

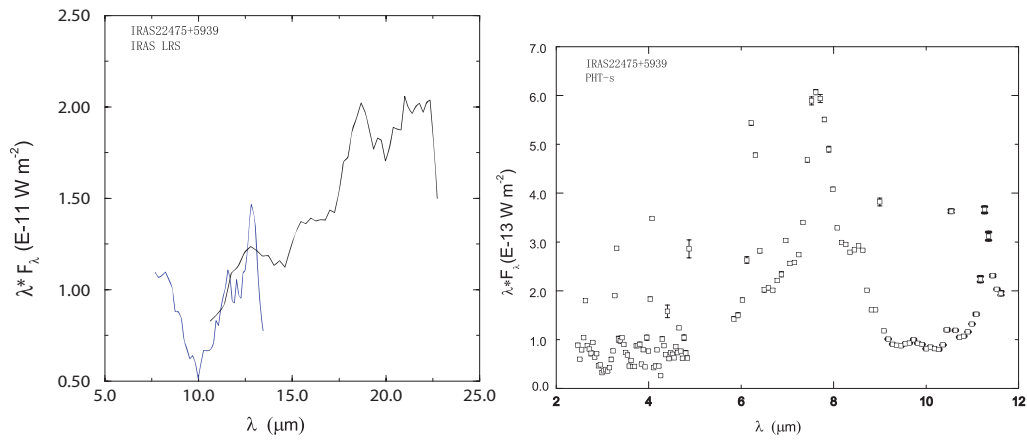


Fig. 6 *Left panel:* the IRAS-LRS spectrum from the LRS database at the University of Calgary, consisting of two wavelength bands: 7.7 – 13.4 μm and 11.0 – 22.6 μm . *Right panel:* the PHT-s spectrum lying in the 2 – 12 μm range.

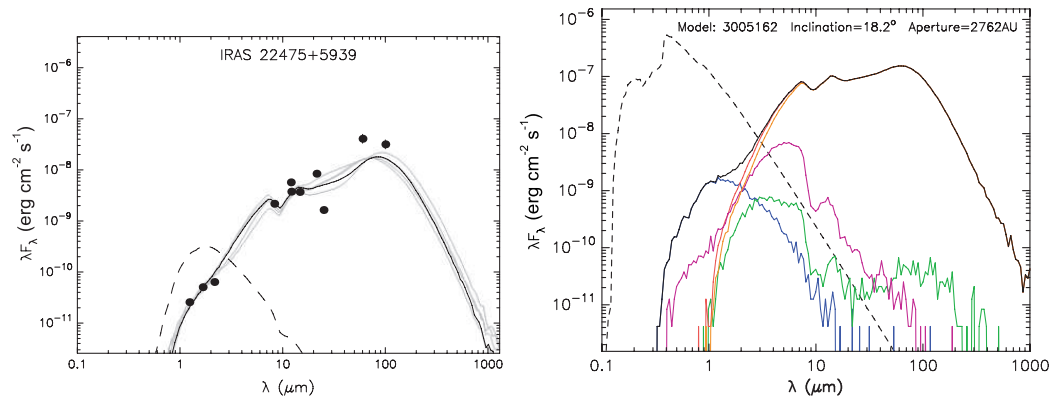


Fig. 7 *Left panel:* the SED of the IRAS 22475+5939 source. The filled circles show the data from 2MASS (*JHK*), MSX (*ACDE*) and IRAS (12, 25, 60, 100 μm). The continuous line shows the best fit model, and the gray lines show subsequent good fits for $(\chi^2 - \chi_{\text{bestfit}}^2)$ per data point < 3 . The dashed line corresponds to the stellar photosphere for the central source of the best fitting model, as it would look in the absence of the circumstellar extinction (but including interstellar extinction). *Right panel:* the various emission disc components making up this model; see text for details. It should be noted that the circumstellar disc (green curve) is important for wavelengths between 1 and 10 μm .

It is apparent from the latter modeling that the central star and disc components of emission are responsible for the MIR/NIR emission, but envelope fluxes are the most important at $\lambda > 10 \mu\text{m}$.

3.6 Discussion

The morphology of the cores is firstly shown from the lines $\text{CO } J = 2 - 1$, $^{13}\text{CO } J = 2 - 1$ and $^{13}\text{CO } J = 3 - 2$, as well as the corresponding parameters. Compared with the results in CO, ^{13}CO and $^{18}\text{CO } J = 1 - 0$ (Guan et al. 2008), the V_{LSR} and the derived physical parameters show little

Table 5 Results from the SED Fitting

Parameter	SM (M_{\odot})	Age (yr)	T_{eff} (K)	DM (M_{\odot})	Disc accretion rate ($M_{\odot} \text{ yr}^{-1}$)	Luminosity L_{\odot}	A_v
Best fit values	15.34	1.54×10^4	9995.8	0.13	1.56×10^{-5}	1.54×10^4	4.53

Notes: SM is short for stellar mass, DM is for disc mass, the luminosity is the total luminosity of the star, and A_v is the foreground extinction. The best fit values are derived from the average values for the best 10 models.

difference, and the structure of $^{13}\text{CO } J = 1 - 0$ that is detected by them is similar to $^{13}\text{CO } J = 2 - 1$. The outflow traced by $\text{CO } J = 2 - 1$ is more extended than that of $\text{CO } J = 3 - 2$ (Jiang et al. 2001). Yang & Wu (1998) only analyzed the IRAS data and discovered that IRAS 22475+5939 may be a massive YSO with high luminosity. Due to the SED in the infrared bands, we suggest that IRAS 22475+5939 is likely to be a class I YSO with mass $15.34 M_{\odot}$, luminosity $1.54 \times 10^4 L_{\odot}$, age 1.54×10^4 yr and T_{eff} 9995.8 K. Its foreground extinction is about 4.53 mag. Jourdain de Muizon et al. (1990) suggest the PAH characteristics are at 7.7, 8.6 and 11.3 μm , the silicate absorption features are at 9.7 μm and the prominent emissions are at 12.8 μm ([NeII]), 15.55 μm ([NeIII]) and 18.7 μm ([SIII]), according to the IRAS-LRS spectrum. However, we combine the IRAS-LRS spectrum with the PHT-s spectrum and find that the PAH emissions are shown at all PAH bands, especially at the main PAH bands (3.3, 6.2, 7.7, 8.6, 11.2 μm) and 16.4 – 17.4 μm . This indicates the diverse PAH family in the molecular cloud. The HII region is likely to be excited by the IR1-an O7V-O7.5V star (Eiroa et al. 1981). Its position almost coincides with IRAS 22475+5939. Therefore, it is possible that the star drives the outflow. It is necessary to have high-resolution observations to identify their relationship.

4 CONCLUSIONS

We observed the IRAS 22475+5939 source using three spectral lines $\text{CO } J = 2 - 1$, $^{13}\text{CO } J = 2 - 1$ and $^{13}\text{CO } J = 3 - 2$. Their V_{SLR} are almost the same, and we further verified the massive, energetic outflow, showing that this region is a high-mass star formation region. The integrated intensity maps of the cores tell us that the molecular cloud is isolated, and that the mass of the core is larger than low-mass cores. The intensity ratio $R_{\text{I}_{32/21}}$ map indicates that gas temperature varies at different positions, and that the maximum value is larger than one, which is bigger than the regions without HII regions (Wilson et al. 1997). In addition, the peaks of the intensity ratio are at the edge of the HII region. This may be because the HII region blows away the hot molecular gas from the center to the edge and heats the gas, which causes the temperature to become higher at the edge than at the center of the molecular core. A higher J transition in ^{13}CO traces the warm regions. PAH features are demonstrated in the Spitzer IRAS 8 μm emission and the spectra of IRAS-LRS and PHT-s, suggesting a rich PAH molecule in the cloud. IRAS 22475+5939 may be a massive, luminous class I protostar with an active disc, but considering the position of the excited star in the HII region, the excited star is able to drive the outflow. This could be the driving source of the outflow. High-resolution observations are needed for better results.

Acknowledgements We would like to thank Drs. Sheng-Li Qin and Martin Miller for the data acquisition. This research has made use of the data products from the 1.4 GHz NRAO VLA Sky Survey (NVSS), and also used the NASA/IPAC Infrared Science Archive, which is operated by the Jet Propulsion Laboratory, California Institute of Technology, under contract with the National Aeronautics and Space Administration. IRAS, MSX and 2MASS photometry were downloaded from NASA/IPAC Infrared Science. We thank SUN Kwok for providing the LRS database at the University of Calgary. The ISOPHOT data were obtained from the ISO Data Archive (IDA); thanks to D. Lemke for reducing the PHT-s data.

References

- Beichman, C. A., Neugebauer, G., Habing, H. J., Clegg, P. E., & Chester, T. J. 1988, in *Infrared Astronomical Satellite (IRAS) Catalogs and Atlases, Explanatory Supplement*, 1
- Beuther, H., Kramer, C., Deiss, B., & Stutzki, J. 2000, *A&A*, 362, 1109
- Blair, G. N., Davis, J. H., & Dickinson, D. F. 1978, *ApJ*, 226, 435
- Bonnell, I. A., Bate, M. R., & Zinnecker, H. 1998, *MNRAS*, 298, 93
- Chen, P. S., Gao, H., & Xiong, G. Z. 1995, *ApJS*, 100, 389
- Churchwell, E. 2002, *ARA&A*, 40, 27
- Deharveng, L., Zavagno, A., Salas, L., et al. 2003, *A&A*, 399, 1135
- Deharveng, L., Zavagno, A., & Caplan, J. 2005, *A&A*, 433, 565
- Dickman, R. L. 1978, *ApJS*, 37, 407
- Eiroa, C., Neckel, T., Sanchez Magro, C., & Selby, M. J. 1981, *A&A*, 95, 206
- Felli, M., & Harten, R. H. 1981, *A&A*, 100, 42
- Garden, R. P., Hayashi, M., Hasegawa, T., Gatley, I., & Kaifu, N. 1991, *ApJ*, 374, 540
- Guan, X., Wu, Y., & Ju, B. 2008, *MNRAS*, 391, 869
- Guan, X., & Wu, Y.-F. 2008, *ChJAA (Chin. J. Astron. Astrophys.)*, 8, 230
- Henkel, C., Guesten, R., & Haschick, A. D. 1986, *A&A*, 165, 197
- Heyer, M. H., Snell, R. L., Morgan, J., & Schloerb, F. P. 1989, *ApJ*, 346, 220
- Hodge, T. M., Kraemer, K. E., Price, S. D., & Walker, H. J. 2004, *ApJS*, 151, 299
- Jiang, L. J., Wu, Y. F., & Miller, M. 2001, *China Academic Journal*, 46, 18
- Jourdain de Muizon, M., Cox, P., & Lequeux, J. 1990, *A&AS*, 83, 337
- Kwok, S., Volk, K., & Bidelman, W. P. 1997, *ApJS*, 112, 557
- Lang, K. R. 1980, *Science*, 207, 174
- Leger, A., & Puget, J. L. 1984, *A&A*, 137, L5
- Lemke, D., Klaas, U., Abolins, J., et al. 1996, *A&A*, 315, L64
- Lockman, F. J. 1989, *ApJS*, 71, 469
- Peeters, E. 2011, in *EAS Publications Series*, vol. 46, eds. C. Joblin, & A. G. G. M. Tielens, 13
- Qin, S.-L., Wang, J.-J., Zhao, G., Miller, M., & Zhao, J.-H. 2008, *A&A*, 484, 361
- Robitaille, T. P., Whitney, B. A., Indebetouw, R., & Wood, K. 2007, *ApJS*, 169, 328
- Scoville, N. Z., Sargent, A. I., Sanders, D. B., et al. 1986, *ApJ*, 303, 416
- Shu, F. H., Adams, F. C., & Lizano, S. 1987, *ARA&A*, 25, 23
- Varricatt, W. P. 2012, *arXiv:1202.4795*
- Volk, K., Kwok, S., Stencel, R. E., & Brugel, E. 1991, *ApJS*, 77, 607
- Wang, J. 1997, Ph. D. thesis (Massachusetts Institute of Technology)
- Wilson, C. D., Walker, C. E., & Thornley, M. D. 1997, *ApJ*, 483, 210
- Wu, Y., Zhang, Q., Chen, H., et al. 2005, *AJ*, 129, 330
- Xu, J.-L., & Wang, J.-J. 2010, *RAA (Research in Astronomy and Astrophysics)*, 10, 151
- Yang, C., & Wu, Y. 1998, *Acta Astrophysica Sinica*, 18, 323
- Zhang, Q., Hunter, T. R., Sridharan, T. K., & Ho, P. T. P. 2001, in *American Astronomical Society Meeting Abstracts, Bulletin of the American Astronomical Society*, 33, #134.13
- Zuckerman, B., & Evans, N. J., II 1974, *ApJ*, 192, L149